COMMUNICATIONS IN SCIENCE AND TECHNOLOGY
Homepage: cst.kipmi.or.id

The effect of synthesis temperature on structural, morphological, and band gap energy of plate-like $Bi_4Ti_{2.95}V_{0.05}O_{12}$ prepared by molten NaCl/KCl salt method

Kanty Maryani[a], Nelly Safitri Anwari[a], Widiya Nur Safitri[b], Arie Hardian[c], Ervina Dwi Inggarwati[a], Anton Prasetyo[a,*]

[a]*Department of Chemistry, Universitas Islam Negeri Maulana Malik Ibrahim Malang, Malang 65144, Indonesia.*
[b]*Department of Chemistry, Institut Teknologi Sepuluh Nopember, Surabaya 60111, Indonesia*
[c]*Department of Chemistry, Universitas Jenderal Achmad Yani, Cimahi, 40531, Indonesia*

Article history:
Received: 22 September 2023 / Received in revised form: 21 December 2023 / Accepted: 13 May 2024

Abstract

Vanadium (V)-doped $Bi_4Ti_3O_{12}$ compound is reported to have good photocatalyst properties; however, efforts still need to improve the ability of the photocatalyst through various strategies, such as controlling the morphology and particle size. The molten salt method is one of the simple synthesis methods reported successful in synthesizing $Bi_4Ti_3O_{12}$ compounds with plate-like/sheet morphology and reported having good photocatalyst activity. One of factor influenced to particle compound obtained by molten salt method is synthesis temperature. Therefore, in this work, V-doped $Bi_4Ti_3O_{12}$ ($Bi_4Ti_{2.95}V_{0.05}O_{12}$) was prepared through the molten salt NaCl/KCl method at various synthesis temperatures: 700, 750, and 800˚C and the effect of temperature synthesized on (a) structural (b) morphological, and (c) band gap energy were studied. These studies used *X*-ray diffraction data (diffractogram), scanning electron microscope (SEM) and diffuse reflectance ultraviolet-visible spectroscopy. The diffractograms showed that the target compound was successfully obtained at all temperature synthesis. The crystallographic data indicated that temperature synthesis determined the lattice parameter values. However, there are no clear trend changes that is possibly due to changes in the valence of the V atom. The synthesis temperature also causes increasing the crystallite size but does not affect the crystallinity samples. SEM images showed that all samples had plate-like/sheets morphology and the particle size became larger at higher temperature. It indicated that the particle growth rate was faster than nucleation rate. Meanwhile, the result of Kubelka-Munk calculation showed that all samples had relatively same band gap energy value (E_g(1) was ~ 2.90, and E_g(2) was ~1.85 eV.

Keywords: Vanadium-doped $Bi_4Ti_3O_{12}$; molten salt method; synthesis temperature

1. Introduction

$Bi_4Ti_3O_{12}$ is one of the tri-layer Aurivillius compound families reported to have a good photocatalytic activity in degrading dye organic waste with a band gap energy of 2.91 eV (426 nm) [1]. Furthermore, applying the $Bi_4Ti_3O_{12}$ compound as photocatalyst material can be more advantageous if it can work at a wider spectrum of wavelengths visible light. It is well known that doping metal element to photocatalyst compound can decrease the band gap energy. Previous studies reported that $Bi_4Ti_3O_{12}$ doped by a metal element such as La, Nd, Fe, Cr, and V metals can decrease the band gap energy [1-2]. Several studies reported that the utilization of vanadium metal as photocatalyst material dopant can decrease the band gap energy [1,3]. Gu, et al. synthesized the compound $Bi_4V_{3x}Ti_{3-3x}O_{12}$ (x = 0, 0.05 and 0.1) through hydrothermal method, and reported the band gap energy of compounds: (a) x=0 was 2.91 eV (426 nm), (b) x= 0.05 was 2,67 eV (464 nm) and (c) x= 0.1 was 2.37 eV (523 nm) [1]. It indicated that the higher concentration of vanadium dopant can cause the decrease in the band gap; as a result, it can work in the visible light region. The vanadium (V) dopant can reduce the band gap energy by forming electronic energy levels below the conduction band involving the *d* orbital of V atom [4].

The morphology and particle size of photocatalyst compounds determine photocatalytic activity [5-7]. The uniformity of particle size and shape morphology can increase the quantum efficiency of interfacial charge transfer; as a result, it prevents e^-/h^+ recombination and increases the absorption of light, thus making the photocatalytic activity better [8]. In addition, Li and Liu suggested that the morphology/shape particle determined the photo-oxidation activity in photocatalyst mechanism [9]. Previous other studies also

* Corresponding author.
Email: anton@kim.uin-malang.ac.id
https://doi.org/10.21924/cst.9.1.2024.1279

reported that $Bi_4Ti_3O_{12}$ compound with a plate-like/sheet morphology had good photocatalyst activity [8,10]. However, Liu et al. reported that Fe-doped $Bi_4Ti_3O_{12}$ compound with a microsphere morphology had a very good ability to degrade methylene blue [5]. Thereof, the synthesis of $Bi_4Ti_3O_{12}$ compound with its typical morphology (plate-like/sheet/microsphere) provides an advantage to increase the photocatalytic activity.

One synthesis method reported to have tuning particle morphology ability is molten salt method. This method uses salt fluxed as a medium to facilitate the precursor's reaction and consists of two main mechanisms i.e. (a) the template-growth, and (b) dissolution-precipitation mechanisms. The template-growth mechanism involves the dissolved reactant in the molten salt diffuses to the surface of the lower soluble reactant, whereas in the dissolution-precipitation mechanism two reactants are completely dissolved in the salt and react to form the product phase [11-13].

The synthesis of the plate-like/sheet $Bi_4Ti_3O_{12}$ compound by molten salt method has been reported by previous researchers [14-15]. Zhao, et al. synthesized $Bi_4Ti_3O_{12}$ by molten salt method using Na_2SO_4/K_2SO_4 salts with synthesis temperature in the range of 850-950^{o}C and obtained the products with plate-like (sheets) morphology [15]. Meanwhile, Agustina, et al. reported the synthesis of vanadium-doped $Bi_4Ti_3O_{12}$ compounds using NaCl salt and impurities $BiNaO_3$ and NaV_6O_{11} were still obtained, while the obtained particle morphology was plate-like/sheet [16]. These studies showed that the molten salt method could provide an opportunity to obtain $Bi_4Ti_3O_{12}$ material with a plate-like/sheet morphology.

There are many determining factors on molten salt method, including (a) salt type, (b) synthesis temperature, (c) synthesis time, and (d) salt to oxide ratio [15, 17-18]. Zhao, et al. reported that the temperature of molten salt synthesis of $Bi_4Ti_3O_{12}$ affected the growth particles and the higher calcination temperature produced the larger particle size [15]. In addition, Marela, et al. synthesized the $Bi_4Ti_3O_{12}$ compound using NaCl salts at synthesis temperature in the range of 800-950^{o}C, and reported that the particle size became larger with the increasing temperature caused by the particle growth rate faster than the nucleation rate [19]. It showed that the temperature of molten salt synthesis had an effect on the particle size growth. On other hand, Gu et al. synthesized vanadium doped $Bi_4Ti_3O_{12}$ ($Bi_4V_{3x}Ti_{3-3x}O_{12}$ (x = 0, 0.05 and 0.1)) compound using the hydrothermal method and the shape of obtained particle were plate-like. They also reported that the V doped $Bi_4Ti_3O_{12}$ had a good photocatalytic activity [1]. Meanwhile, Handayani et al. reported the synthesized V doped $Bi_4Ti_3O_{12}$ using molten salt method and the obtained particle shape was plate-like [3]. However, a specific study of the effect of synthesis temperature on the V-doped $Bi_4Ti_3O_{12}$ particle prepared by the molten salt method has still never been reported especially the one using the mixed salt of NaCl/KCl. Meanwhile, using mixed salts provides an advantage by allowing synthesis at lower temperatures [18]. Therefore, in this work, the V-doped $Bi_4Ti_3O_{12}$ compound ($Bi_4Ti_{2.95}V_{0.05}O_{12}$) was synthesized using the molten mixed NaCl/KCl salt method with various temperatures and the effects of synthesis temperature on (a) structure, (b) morphology, and (c) band gap energy were studied.

2. Materials and Methods

2.1. Materials

The materials used in this study included bismuth (III) oxide (Bi_2O_3, Himedia, 99.9% powder), titanium dioxide (TiO_2, Aldrich, 99.9% powder), vanadium (III) oxide (V_2O_3, Sigma Aldrich, 99.5% powder), sodium chloride (NaCl, Merck, 99.5% powder), potassium chloride (KCl, Merck, 99.5% powder), acetone (Merck), and silver nitrate ($AgNO_3$, Merck, Powder).

2.2. Methods

In this study, the V-doped $Bi_4Ti_3O_{12}$ compound ($Bi_4Ti_{2.95}V_{0.05}O_{12}$/BTVO) was obtained by molten salt method using mixed NaCl/KCl salt with mol ratio 1:1. Precursor and salt requirements were calculated stoichiometrically. BTVO synthesis was carried out by mixing the precursors Bi_2O_3, TiO_2 and V_2O_3, which were adjusted based on stoichiometric calculations. The sample product and the mixed salt of NaCl/KCl with the ratio of 1:7:7 were crushed using agate mortar for 1 hour and added with acetone to homogenize the mixture. In this study, three samples were prepared and calcined at (a) 700°C (BTVO-700), (b) 750°C (BTVO-750) and (c) 800°C (BTVO-800) for 6 hours. The synthesized samples were removed from the furnace and rinsed with hot distilled water for several times to remove the mixed salt used. The remaining NaCl/KCl salts were identified by dripping $AgNO_3$ to the filtrate. Then, all samples were heated in oven at 90°C for 3 hours.

2.3. Characterization

The samples were characterized using *X*-ray diffraction (Rigaku Miniflex diffractometer, Japan) to determine the phase structure of samples. The measurements were conducted at 2θ (°) = 10-90 in which step size measurement was 0.02^o. The diffractogram samples were refined with Rietica software using Le-Bail method. The highest intensity of diffractogram peak was used to calculate the crystallite size of the sample using Equation 1 (the Debye-Scherer Equation).

$$D = \frac{K\,\lambda}{\beta\,Cos\,\theta} \quad (1)$$

D is the crystallite size (nm), K is the Scherer constant (0.9), β is full-width half maximum peak (radians), λ is the wavelength of X-ray source with Cu k-α (1.5406 nm), and θ is diffraction angle [20].

Scanning electron microscope-Energy dispersive *X*-ray spectroscopy characterization used Jeol JSM-6510, Japan. The SEM images obtained were processed using Image-J software to determine the particle size. In addition, the EDS spectrum was used to analyze the composition of the constituent elements of the samples. Ultraviolet-visible diffuse reflectance spectroscopy (Thermo Scientific Evolution 220 spectrometer, USA) measurement was conducted at a range wavelength: 200-800 nm. The reflectance spectrum was calculated using Kubelka-Munk (Equation 2) to obtain the band gap energy.

$$F(R) = \frac{(1-R)^2}{2R} = \frac{K}{S} \quad (2)$$

F(R) is Kubelka-Munk factor, *K* is molar absorption coefficient, *S* is scattering coefficient, and *R* is reflectance measured value. The band gap energy was calculated by linear regression at the value of *x* (*hv* = band gap energy) at *y*= 0 [21].

3. Results and Discussion

Fig. 1 shows the diffractogram of BTVO samples and it can be seen that the diffractogram samples had a similar pattern to the diffractogram standard of $Bi_4Ti_3O_{12}$ (The Inorganic Crystal Structure Database/ICSD 159929) indicating that $Bi_4Ti_{2.95}V_{0.05}O_{12}$ compound was successfully synthesized. Fig. 1 also shows that no other peaks indicating that the impurities did not form. All diffractograms were refined by the Le-Bail method (using the diffractogram standard of $Bi_4Ti_3O_{12}$ on ICSD 159929). The refinement plots are shown in Fig. 2, and the result data are summarized in Table 1, showing that the R_p and R_{wp} values for all samples were below 10. It indicated that the sample diffractograms had a high agreement with the diffractogram standard [22].

Fig. 3 shows the shifting peak position at the highest diffractogram intensity ($2\theta = 30.05^\circ$), and it can be seen that the peak of BTVO-700 and BTVO-750 shifted to the bigger position. It corresponded to a change in lattice size due to the partially small Ti atoms being replaced with vanadium dopant resulting in a change in the length of the *B*-O bond. In this research, V_2O_3 precursors were used; hence, the valence of the vanadium atoms was 3. However, the use of high temperatures in this research could lead to the changes in the valence of the atoms [23]. Therefore, there was a possibility of a change in the valence of the V atom into pentavalent (V^{5+}). The change in bond length in BTVO-700 as well as BTVO-750 was related to the ionic radii of V^{5+} (0.54 nm) smaller than Ti^{4+} (0.605 nm) [24]. Fig. 3 also shows that the peak position of the BTVO-800 that was relatively the same as standard data. It indicated that the V atom valence was probably unchanged (ionic radii of V^{3+} is 0.64 nm [24]). Therefore, the lattice size did not change. The crystallographic data obtained from the refinement process also indicated changes in the lattice parameters (*a*, *b*, and *c*), but there was no trend and it may correlate to changes in the valence of the V atom. However, *X*-ray photoelectron spectroscopy measurement was not conducted; therefore, providing a more detailed explanation is somewhat challenging.

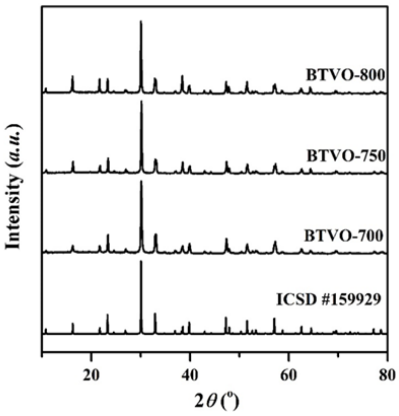

Fig. 1. Diffractograms of BTVO-700, BTVO-750, and BTVO-800 samples

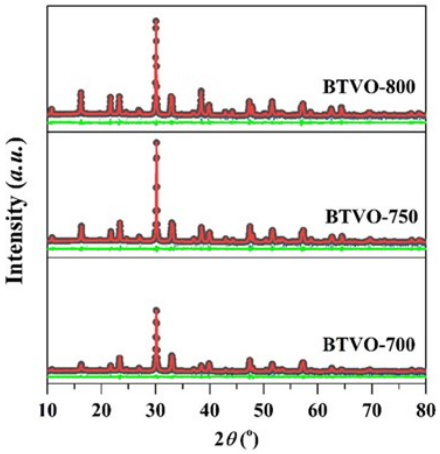

Fig. 2. The refinement plots of BTVO-700, BTVO-750, and BTVO-800

Table 1. The results of refinement data

Parameter	BTVO-700	BTVO-750	BTVO-800
Crystal system	Orthorhombic	Orthorhombic	Orthorhombic
Space group	*B2cb*	*B2cb*	*B2cb*
Z	4	4	4
a (Å)	5.46213(4)	5.44512(0)	5.45161(4)
b (Å)	5.42011(3)	5.41025(1)	5.41236(0)
c (Å)	32.94081(3)	32.78873(1)	32.80612(6)
Cell volume (Å^3)	975.2(1)	965.94(9)	967.98(7)
R_p (%)	9.41	8.92	8.61
R_{wp} (%)	6.57	6.34	6.65
GoF (%)	0.15	0.16	0.17

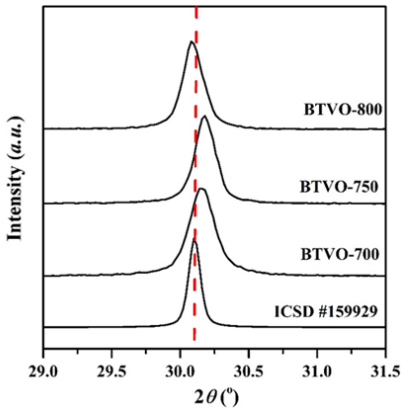

Fig. 3. Diffractogram peak at $2\theta = 30.05^\circ$

Table 2. The crystallite size of BTVO

Sample	Crystallite size (nm)
BTVO-700	38.07
BTVO-750	46.55
BTVO-800	46.57

The calculation of crystallite size used the highest intensity of the diffractogram peaks at $2\theta = 30.05^\circ$, and the results are summarized in Table 2. The results showed that the sample synthesized using a higher temperature had a larger crystallite

size as the higher temperature could give bigger energy supplied as a result of the increasing dissolution rate and then raising the rate of crystallite size growth [25,26]. The difference in crystallite size between the BTVO-700 and BTVO-750 samples was quite significant indicating the crystallite size growth rate raised significantly due to increasing temperature. However, the BTVO-800 sample had a crystallite size that was relatively the same as BTVO-750. It was probably related to the concept "the growth dead zone", or the crystals no longer could grow even on a supersaturated condition [27]. All diffractograms had a sharp shape that indicated that all samples had good crystallinity. In addition, the diffractogram of the sample synthesized at the lowest temperature (BTVO-700) did not find any impurity. It showed that the lowest synthesis temperature 700°C was sufficient to facilitate the reaction between precursors.

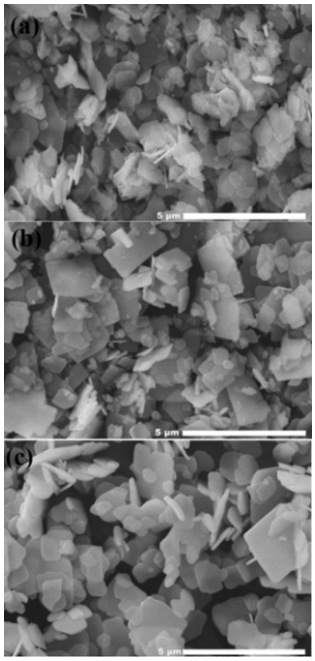

Fig. 4. Micrograph of (a) BTVO-700, (b) BTVO-750, and (c) BTVO-800

Fig. 4 shows the micrograph of BTVO compounds, and it can be seen that BTVO particles had a plate-like morphology. It is well known that the plate-like morphology is a typical morphology of the Aurivillius compound synthesized using the molten salt method [15,28-29]. The micrograph also shows no agglomeration and aggregation particles in all samples indicating that the synthesis temperature did not affect the morphology of the particles. As shown in Fig. 5, the particle size distribution of the sample was calculated using Image J software. Table 3 summarizes the particle size averages showing that the particle size became larger as the synthesis temperature increased. Marella, et al. suggested that the particle growth stage in the molten salt method includes (a) nucleation (reactant particles reacting to each other in the molten salt to form product particle nuclei) and (b) crystal growth (crystal nuclei reacting to form a greater matrix) [17]. The particle size of the BTVO-800 sample was found at the largest, which indicated that the crystal growth rate was faster. The fast crystal growth rate at high temperatures caused the surface energy increasing; therefore, the particles would diffuse and combine to form larger particles to reduce its surface energy [11,30]. In addition, higher temperatures caused the diffusion rate between atoms to accelerate, thereby making the growth of particles larger. It then made the obtained particle larger [19]. Table 4 presents the results of energy dispersive *X*-ray spectroscopy spectrum, showing the element content of the BTVO compound.

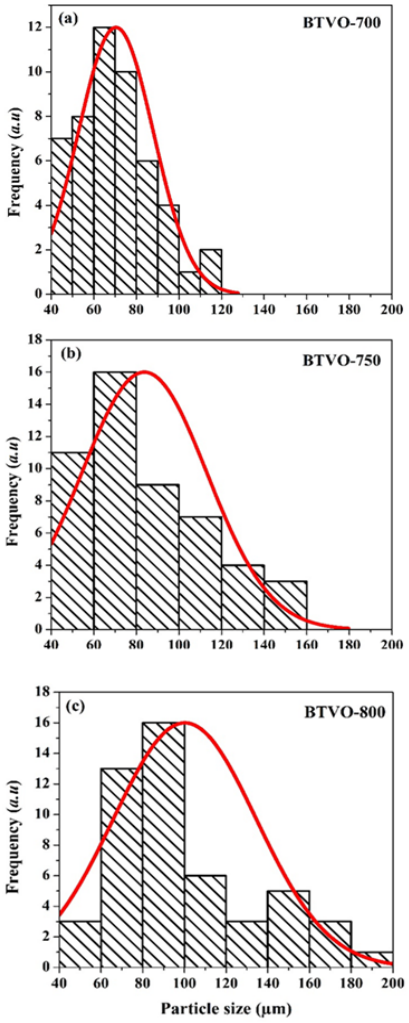

Fig. 5. Particle size distribution of BTVO

Table 3. The average particle size of BTVO

Sample	Average particle size (μm)
BTVO-700	70.372
BTVO-750	83.736
BTVO-800	100.198

Table 4. The elements composition in BTVO samples

Element (%weight)	BTVO-700	BTVO-750	BTVO-800
Oxygen	20.81	24.99	21.32
Bismuth	62.01	58.08	61.63
Titanium	16.11	15.55	16.03
Vanadium	1.07	1.38	1.02

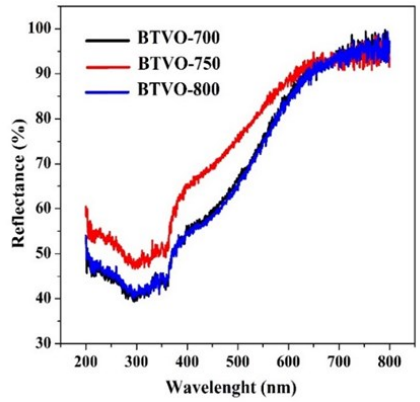

Fig. 6. The reflectance spectra of BTVO

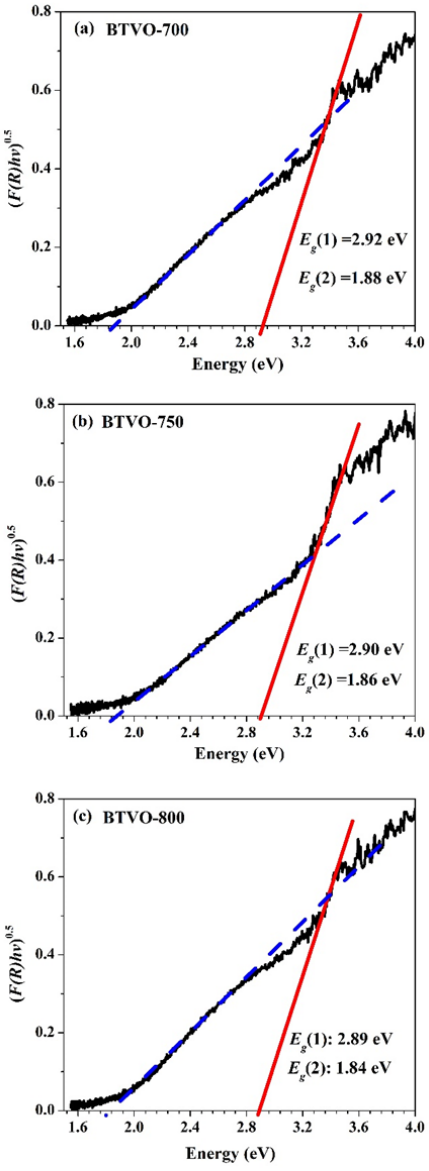

Fig. 7. Plot-tauc of BTVO

Fig. 6 and Fig. 7 show the UV-Vis DRS reflectance spectra of BTVO compound, and the Tauc plot for calculating the band gap energy, respectively. Table 5 meanwhile provides a summary of the results of the band gap energy calculation. As seen in Fig. 7, the BTVO compound had two distinct adsorption edges in the region around (a) ~428, and (a) ~670 nm. This result was similar with the one reported by Ramana, et al. (2017) that suggested that the $Bi_4Ti_3O_{12}$ compound doped with samarium and vanadium had two distinct adsorption edges at around 400 and 600 nm [31]. The first band gap energy value (~2.90 eV) was relatively the same as the one reported by Liu, et al. and involved electrons in the Bi-6*s* + O-2*p* orbitals in the valence band and Ti-3*d* in the conduction band [32]. In addition, the first band gap energy value also was similar with the one reported by Gu, et al. for undoped $Bi_4Ti_3O_{12}$ (2.9 eV) [1]. Meanwhile, the second band gap energy had a lower value due to the substitution of V on the Ti atom in $Bi_4Ti_3O_{12}$ material, and it caused the formation of a new electronic band sub-structure [31]. The substitution of V was more electronegative than Ti; therefore, an interstitial state was formed by the V orbital in 3*d*, located at the bottom of the Ti-3*d* conduction band [1,33-34].

Table 5. The band gap energy of BTVO

Sample	E_g(1) (eV/nm)	E_g(2) (eV/nm)
BTVO-700	2.92/425	1.88/659
BTVO-750	2.90/428	1.86/667
BTVO-800	2.89/429	1.84/674

The band gap energies of all samples were relatively the same, as tabulated in Table 5. It indicated no effect of particle size on the obtained band gap energy indicating no quantum confinement effect in samples. The absence of the quantum confinement phenomenon was possible since the obtained particle size could not be classified as a nanomaterial [35]. The second band gap energy of BTVO also showed that this compound could work in the visible region (~670 nm/red color), thus providing advantages as a photocatalyst material.

4. Conclusion

The V-doped $Bi_4Ti_3O_{12}$ compound ($Bi_4Ti_{2.95}V_{0.05}O_{12}$) was successfully prepared by the molten mixed NaCl/KCl salt method using the synthesis temperatures at 700, 750 and 800°C. The synthesis temperature affected the parameter lattice and crystallite size of the sample but did not affect the crystallinity of the sample. All samples had similar morphology, i.e. plate-like/sheet; however, the particle size was different, which indicated that the temperatures synthesis affected particle growth rates. The band gap energy obtained had relatively the same value (~2.90 for E_g(1) and ~1.85 eV for E_g(2)), which correlated to the absence of a quantum confinement effect.

Acknowledgements

We thank Department of Chemistry, Faculty Science and Technology, Universitas Islam Negeri Maulana Malik Ibrahim Malang that has supported by providing supporting laboratory facilities.

References

1. D. Gu, Y. Qin, Y. Wen, T. Li, L. Qin, and H.J. Seo, *Electronic structure*

and optical properties of V-doped $Bi_4Ti_3O_{12}$ nanoparticles. Journal of Alloys and Compounds, J. Alloys Compd. 695 (2017) 2224–2231.

2. Y. Liu, et al., *Enhanced photocatalytic activity of $Bi_4Ti_3O_{12}$ nanosheets by $Fe3^+$-doping and the addition of Au nanoparticles: Photodegradation of Phenol and bisphenol A*, Appl. Catal. B: Environ. 200 (2017) 72–82.
3. R. Handayani, W.N. Safitri, N. Aini, A. Hardian, and A. Prasetyo, *Synthesis and characterization of vanadium doped $Bi_4Ti_3O_{12}$ as photocatalyst material*, IOP Conf. Ser.: Mater. Sci. Eng. 578 (2019) 1.
4. H. Bentawal, U.S. Shenoy, and D.K. Bhat, *Vanadium-doped $SrTiO_3$ nanocubes: Insight into role of vanadium in improving the photocatalytic activity*, Appl. Surf. Sci.. 513, (2020) 145858
5. Z. Liu, and Z. Ma, *Promoting the photocatalytic activity of $Bi_4Ti_3O_{12}$ microspheres by incorporating iron*, RSC Adv. 10 33 (2020) 19232–19239.
6. A. Stanković, S. Dimitrijević, and D. Uskoković, *Influence of size scale and morphology on antibacterial properties of ZnO powders hydrothemally synthesized using different surface stabilizing agents*, Colloids Surf. B: Biointerfaces. 102 (2013) 21-28.
7. A.S. Rini, A.P. Aji, and Y. Rati, *Microwave-assisted biosynthesis of flower-shaped ZnO for photocatalyst in 4-nitrophenol degradation*, Commun. Sci. Technol. 7 2 (2021) 135-139.
8. Y. Zhang, J. Gao, Z. Chen, and Z. Lu, *Enhanced photocatalytic performance of $Bi_4Ti_3O_{12}$ nanosheets synthesized by a self-catalyzed fast reaction process,* Ceram. Int., 44 18 (2018) 23014-23023.
9. Y.F., Li, and Z.P. Liu, Particle Size, *Shape and Activity for Photocatalysis on Titania Anatase Nanoparticles in Aqueous*, J. Am. Chem. Soc. 133 (2011) 15743–15752
10. Z. Chen, H. Jiang, W. Jin, and C. Shi, *Enhanced photocatalytic performance over $Bi_4Ti_3O_{12}$ nanosheets with controllable size and exposed {001} facets for Rhodamine B degradation*, Appl. Catal. B: Environ. 180 (2016) 698-706.
11. T. Kimura, *Molten Salt Synthesis of Ceramic Powders. In: Advances in Ceramics-Synthesis and Characterization, Processing and Specific Applications*, Prof Costas Sikalidis (Ed), IntechOpen, 2011 75-100
12. D.A. Austin, M. Cole, M.C. Stennett, C.L. Corkhill, and N.C. Hyatt, *A preliminary investigation of the molten salt mediated synthesis of Gd_2TiO_5 'stuffed' pyrochlore*, MRS Adv. 6 4-5 (2021) 149-153.
13. L.T. Tseng, X. Luo, T.T. Tan, S. Li, and J. Yi, *Doping concentration dependence of microstructure and magnetic behaviours in Co-doped TiO_2 nanorods Nanoscale*, Res. Lett. 9 1 (2014) 1-10.
14. H. He, et al., *Size controllable synthesis of single-crystal ferroelectric $Bi_4Ti_3O_{12}$ nanosheet dominated with {001} facets toward enhanced visible-light-driven photocatalytic activities*, Appl. Catal. B: Environ. 156–157 (2014) 35-43.
15. Z. Zhao, X. Li, H. Ji, and M. Deng, *Formation mechanism of plate-like $Bi_4Ti_3O_{12}$ particles in molten salt fluxes*, Integr. Ferroelectr. 154 1 (2014) 154–158.
16. K.R. Agustina, D. Suheriyanto, and A. Prasetyo, *The moltens salt synthesis of Vanadium doped $Bi_4Ti_3O_{12}$ using single salt NaCl*, Jurnal Kartika Kimia. 3 1 (2020) 19-24.
17. E.K. Akdogan, R.E. Brennan, M. Allahverdi, and A. Safari, *Effects of molten salt synthesis (MSS) parameters on the morphology of $Sr_3Ti_2O_7$ and $SrTiO_3$ seed crystals*, J. Electroceram. 16 2 (2006) 159-65.
18. S.K. Gupta, and Y. Mao, *A review on molten salt synthesis of metal oxide nanomaterials: Status, opportunity, and challenge*, Prog. Mater. Sci. 117 (2021) 100734.
19. S.D. Marella, N. Aini, A. Hardian, V. Suendo, and A. Prasetyo, *The effect of temperature synthesis on the plate-like particle of $Bi_4Ti_3O_{12}$ obtained by single molten NaCl salt,* J. Pure Appl. Chem. 10 1 (2021) 64-71.
20. E.M. Benali, et al., *Effect of synthesis route on structural, morphological, Raman, dielectric, and electric properties of $La_{0.8}Ba_{0.1}Bi_{0.1}FeO_3$*, J. Mater. Sci. Mater. Electron. 31 4 (2020) 3197-3214.
21. P. Makuła P, M. Pacia, and W. Macyk, *How to correctly determine the band gap energy of modified semiconductor photocatalysts based on UV-Vis Spectra*, J. Phys. Chem. Lett. 9 23 (2018) 6814-6817.
22. B.H. Toby, *R factors in Rietveld analysis: How good is good enough?,* Powder Diffr. 21 1 (2006) 67-70.
23. I.N. Cahyo, N. Aini, F.V. Steky, V. Suendo, W.N. Safitri, and A. Prasetyo, *Synthesis of plate-like Fe-doped $SrBi_4Ti_4O_{15}$ using Na_2SO_4/K_2SO_4 molten salt method: XRD, Raman spectroscopy, SEM, and UV–VIS DRS studies*. J. Iran. Chem. Soc. 20 (2023) 3079–3085
24. R. Shannon, *Revised effective ionic radii and systematic studies of interatomie distances in halides and chalcogenides*, Acta Crystallogr. A. 32 5 (1976) 751-767.
25. G. Madras, and B.J. McCoy, *Temperature effects for crystal growth: A distribution kinetics approach,* Acta Mater. 51 7 (2003) 2031-2040.
26. J.P. Zuniga, S.K. Gupta, M. Abdou, and Y. Mao, *Effect of molten salt synthesis processing duration on the photo- and radioluminescence of UV-, Visible-, and X-ray-Excitable $La_2Hf_2O_7:Eu^{3+}$ Nanoparticles*, ACS Omega. 3 7 (2018) 7757-70.
27. Y. Liu, et al., *When crystals do not grow: The growth dead zone,* Cryst. Growth Des. 19 8 (2019) 4579-4587.
28. W. Zhao, Z. Jia, E. Lei, L. Wang, Z. Li, and Y. Dai, *Photocatalytic degradation efficacy of $Bi_4Ti_3O_{12}$ micro-scale platelets over methylene blue under visible light*, J. Phys. Chem. Solids. 74 11 (2013) 1604-7.
29. P. Sari, S.N. Himmah, A. Hardian, N. Aini, and A. Prasetyo, *Synthesis and characterization of plate-like vanadium doped $SrBi_4Ti_4O_{15}$ prepared via KCl molten salt method*, Commun. Sci. Technol. 7 2 (2022) 175-80.
30. L. Luo, S. Wang, H. Wang, C. Tian, and B. Jiang, *Molten-salt technology application for the synthesis of photocatalytic materials,* Energy Technol. 9 2 (2021) 1-14.
31. E.V. Ramana, et al. *Effect of samarium and vanadium co-doping on structure, ferroelectric and photocatalytic properties of bismuth titanate*, RSC Adv. 7 (2017) 9680.
32. Y. Liu, M. Zhang, L, Li and X. Zhang, *One-dimensional visible-light-driven bifunctional photocatalysts based on $Bi_4Ti_3O_{12}$ nanofiber frameworks and Bi_2XO_6 (X = Mo, W) nanosheets*, Appl. Catal. B.Environ. 160-161 (2014) 757-766.
33. A. Kubacka, A. Fuerte, A. Martínez-Arias, and M. Fernández-García, *Nanosized Ti-V mixed oxides: Effect of doping level in the photo-catalytic degradation of toluene using sunlight-type excitation*, Appl. Catal. B: Environ. 74 1-2 (2007) 26–33.
34. M. Khan, Y. Song, N. Chen, and W. Cao, *Effect of V doping concentration on the electronic structure, optical and photocatalytic properties of nano-sized V-doped anatase TiO_2*, Mater. Chem. Phys. 142 1 (2013) 148-53.
35. M. Singh, M. Goyal, and K. Devlal, *Size and shape effects on the band gap of semiconductor compound nanomaterials*. J. Taibah Univ. Sci. 12 4 (2018) 470-475.